



Free State Conformational Sampling of the SAM-I Riboswitch Aptamer Domain

Colby D. Stoddard,¹ Rebecca K. Montange,^{1,4} Scott P. Hennelly,² Robert P. Rambo,³ Karissa Y. Sanbonmatsu,² and Robert T. Batey^{1,*}

¹Department of Chemistry and Biochemistry, University of Colorado at Boulder, UCB 215, Boulder, CO 80309-0215, USA

DOI 10.1016/j.str.2010.04.006

SUMMARY

Riboswitches are highly structured elements residing in the 5' untranslated region of messenger RNAs that specifically bind cellular metabolites to alter gene expression. While there are many structures of ligand-bound riboswitches that reveal details of bimolecular recognition, their unliganded structures remain poorly characterized. Characterizing the molecular details of the unliganded state is crucial for understanding the riboswitch's mechanism of action because it is this state that actively interrogates the cellular environment and helps direct the regulatory outcome. To develop a detailed description of the ligand-free form of an S-adenosylmethionine binding riboswitch at the local and global levels, we have employed a series of biochemical, biophysical, and computational methods. Our data reveal that the ligand binding domain adopts an ensemble of states that minimizes the energy barrier between the free and bound states to establish an efficient decision making branchpoint in the regulatory process.

INTRODUCTION

Riboswitches are *cis*-acting mRNA regulatory elements that modulate gene expression through their ability to bind small molecule metabolites with high specificity (Montange and Batey, 2008; Roth and Breaker, 2009). Ligand binding to a receptor, called the aptamer domain, redirects the folding outcome of the 5'-untranslated region of the mRNA, thereby determining the expression fate of the mRNA (Garst and Batey, 2009). During transcription, the branchpoint of two parallel folding pathways occurs at a point when a sufficient amount of the mRNA has been synthesized and folded such that it can actively interrogate the cellular environment for ligand (Figure 1A) (sensing phase). To be an effective regulator of gene expression, the unliganded state of the riboswitch must maintain ligand-binding competence without negating the ability to follow a default folding pathway in the absence of ligand. As regulatory decisions by

the secondary structural switch are being made, the mRNA likely becomes locked into a single path that can no longer exchange with the other on a timescale relevant to transcriptional regulation (Figure 1A) (regulatory phase). Despite significant progress in understanding how riboswitches recognize their cognate ligand (Montange and Batey, 2008; Roth and Breaker, 2009), their folding pathways and the nature of the unbound state during the sensing phase are not well defined.

Previous studies have presented an inconsistent picture of the apo-form of riboswitches. One perspective arises from the crystal structures of the Thermotoga maritima asd lysine riboswitch in both the apo and bound forms that reveal almost identical structures (Garst et al., 2008; Serganov et al., 2008). Since the binding pocket for lysine is completely solvent inaccessible, this cannot represent the binding competent form, as suggested by SAXS and chemical probing data (Garst et al., 2008; Sudarsan et al., 2003). Conversely, NMR studies of the free and bound form of the Bacillus subtilis queC preQ1 riboswitch indicated that the receptor is largely unstructured in the absence of ligand binding (Kang et al., 2009). It is not clear how the ligand can efficiently recognize such a disorganized binding pocket RNA in a short temporal window during transcription. Finally, the apostate of the guanine riboswitch appears to be somewhere in the middle of these two extremes. Chemical probing analysis of this RNA demonstrated that part of the binding pocket is conformationally restricted prior to ligand binding while other regions remain flexible allowing the RNA to fold around guanine upon an initial docking event to yield the structure observed by X-ray crystallography (Gilbert et al., 2006; Stoddard et al., 2008). This view of a partially organized binding pocket in the guanine/adenine riboswitches is supported by NMR studies (Ottink et al., 2007) and molecular dynamics simulations (Priyakumar and Mackerell, 2009; Sharma et al., 2009; Villa et al., 2009). It is most likely that all of these RNAs adopt an ensemble of rapidly interconverting states in the absence of ligand with only a subpopulation that are competent to bind ligand, as observed in HIV transactivation element (Zhang et al., 2007). However, the molecular details of the ensemble structures of unliganded riboswitches remain elusive.

To develop a molecular-level understanding of the ensemble of states that a riboswitch aptamer domain experiences during the sensing phase, we have analyzed a sequence based upon the *Thermoanearobacter tengcongensis metF-H2* SAM-I riboswitch (Montange and Batey, 2006). This aptamer is found in

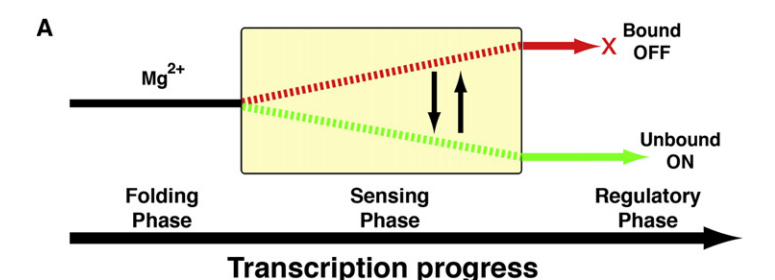
²Theoretical Biology and Biophysics, Theoretical Division, Los Alamos National Laboratory, Los Alamos, NM 87545, USA

³Life Science Division, Lawrence Berkeley National Laboratory, Berkeley, CA 94720, USA

⁴Present address: JILA/NIST, University of Colorado, Boulder, CO 80309-0440, USA

^{*}Correspondence: robert.batey@colorado.edu





varying regulatory contexts including transcriptional and translational control (Barrick and Breaker, 2007) and as a *trans*-acting noncoding RNA that regulates via an antisense mechanism (Loh et al., 2009). Because of the "mix-and-match" nature of riboswitch aptamer and expression platforms (Stoddard and Batey, 2006), analysis of the aptamer domain outside the context of its host RNA yields insights into the general behavior of ligand recognition. The aptamer domain exerts control over surrounding sequence elements rather than the converse. Thus, the reductionist approach required for this study yields biologically relevant insights into the regulatory activity of riboswitches.

The aptamer domain of the SAM-I riboswitch contains a conserved core composed of a secondary structure defined by four helical regions (P1-P4) centered around a four-way junction with three joining regions (J1/2, J3/4, and J4/1) (Figure 1B) (Epshtein et al., 2003; Grundy and Henkin, 1998; Winkler et al., 2003). The helices form two coaxial stacks (P1/P4 and P2/P3) that are organized through a set of tertiary interactions involving a pseudoknot (PK) between L2 and J3/4, a base triple tying together L2, J3/4, and J4/1, and several long-range interactions involving base triples between J1/2 and J3/4 and paired regions (Montange and Batey, 2006) (Figure 1C). S-adenosylmethionine (SAM) recognition is achieved through extensive hydrogen bonding interactions within a pocket created by the minor groove P3 and an electrostatic interaction between the positively charged sulfonium ion on SAM and the minor groove of P1 (Montange and Batey, 2006; Montange et al., 2010).

In this study, we have defined the features of both the folding of the aptamer and its structural flexibility in the absence of SAM. Chemical probing of the RNA revealed that magnesium facilitates formation of a subset of tertiary interactions in the RNA and that SAM is required to establish a protection pattern fully

Figure 1. Regulation and Structure of the SAM-I Riboswitch

(A) Transcription of a nascent riboswitch RNA. The first phase is the synthesis and magnesium-induced folding of the aptamer domain (folding phase). During the second phase, the aptamer interrogates the cellular environment for the presence of SAM (sensing phase). The final phase (regulatory phase) occurs after sufficient downstream sequence has been synthesized to allow for formation of secondary structural elements that direct the expression machinery.

(B) Structure of the SAM-I aptamer domain used in this study, highlighting key tertiary interactions including the 24/64/85 base triple, pseudoknot interaction (PK), and the kinkturn (KT).

(C) Crystal structure of the SAM-I aptamer in complex with SAM, colored according to the secondary structure (PDB ID 2GIS).

consistent with the crystal structure. These data suggest that the folded but unliganded RNA exists as an ensemble of states. In this ensemble, we identified conformations using small angle X-ray scattering (SAXS) that are variable in the degree in which P1 and P3 "scissor" apart from each other allowing formation of multiple open orientations as well as a bound-like state with P1 and P3 in

a closed orientation. Conformational heterogeneity is also observed at the local level within the SAM-binding pocket, as revealed by a crystallographic analysis of the free state along with replica exchange molecular dynamics (REMD) simulations. This study presents a comprehensive understanding of structural heterogeneity in a free state riboswitch aptamer domain and how magnesium and SAM binding reshape the folding land-scape.

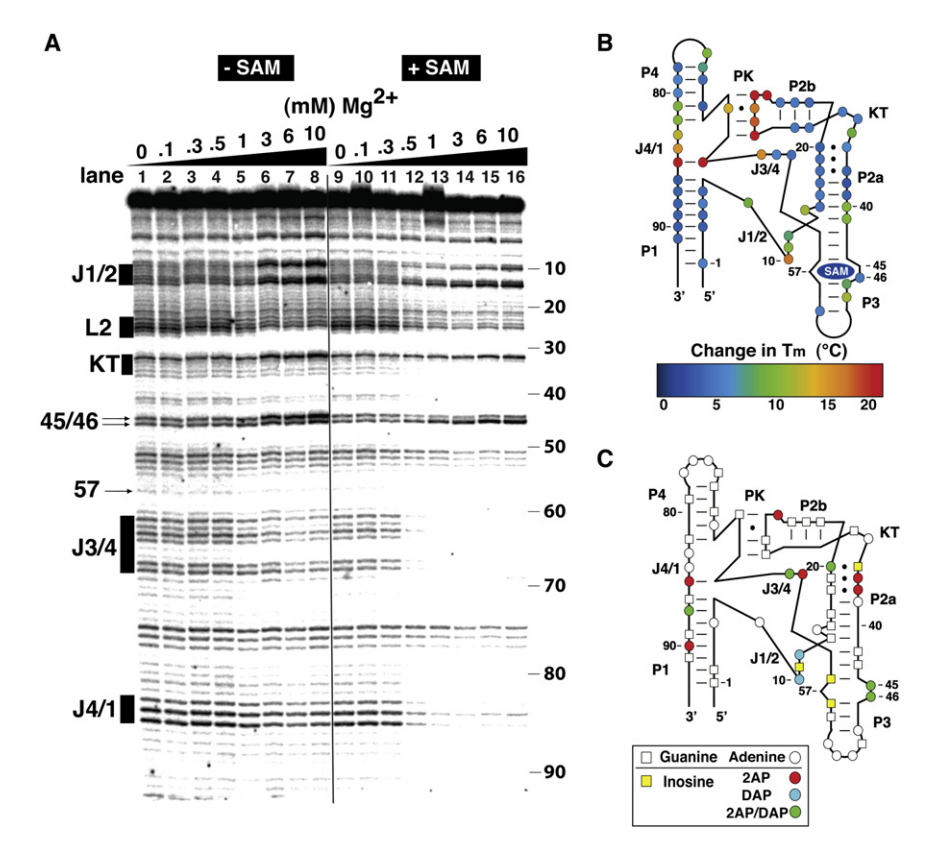
RESULTS

Magnesium and SAM Binding Alter Aptamer Domain Conformational Sampling

To characterize magnesium- and SAM-dependent acquisition of tertiary architecture in the SAM-I riboswitch aptamer domain with nucleotide resolution, we utilized a chemical probing technique called selective 2'-hydroxyl acylation analyzed by primer extension (SHAPE) (Merino et al., 2005; Wilkinson et al., 2006). This approach employs *N*-methylisatoic anhydride (NMIA) as a probing reagent that selectively modifies 2'-hydroxyl groups within regions where the backbone is conformationally flexible (Gherghe et al., 2008). Conversely, nucleotides that are locked in helices or highly structured tertiary elements display low chemical reactivity.

SHAPE analysis was performed at a fixed temperature (20°C) over a range of magnesium concentrations (0–10 mM) in the presence and absence of SAM (Figure 2A). In the absence of SAM (Figure 2A, lanes 1–8), the RNA undergoes multiple magnesium-induced structural transitions. The first folding transition is observed in the pseudoknot between 0.5 and 1 mM MgCl₂, followed by an increased reactivity of positions 9 and 14 in J1/2 between 1 and 3 mM MgCl₂. The increased modification in J1/2 is likely due to folding events that permit sampling of





a bound-like conformation in which positions 9 and 14 are solvent exposed as observed in the crystal structure (Montange and Batey, 2006). Acquisition of other features characteristic of the folded, SAM-bound state are observed in the kink-turn, J3/4, and J4/1, which all display increasing levels of protection

at higher magnesium concentrations but do not appear to

become fully protected at 10 mM MgCl₂.

Since chemical probing reports the bulk ensemble RNA folding behavior, the observed pattern of magnesium-dependent protections reflects the population sampling conformations associated with varying degrees of tertiary architecture formation. In the presence of SAM (Figure 2A, lanes 9-16), almost the entire RNA becomes protected from modification over a narrow magnesium concentration range (0.5-1 mM MgCl₂). Furthermore, in a manner distinct from modification patterns in the absence of ligand, a complete population shift from the free to bound state modification signature occurs in the pseudoknot and J1/2 as well as in the kink-turn, J3/4, and J4/1, suggesting these elements rarely sample structures lacking formation of tertiary architecture in the presence of SAM. This demonstrates that at physiological magnesium concentrations (0.5-1 mM), magnesium and SAM binding is coupled to fully stabilize the tertiary structure of the aptamer, as has been observed previously (Heppell and Lafontaine, 2008; McDaniel et al., 2005).

Temperature-dependent folding of the RNA was monitored in a similar fashion by probing at constant magnesium (6 mM MgCl₂) over a broad temperature range (20-70°C) (see Figure S1 available online). The extent of modification, determined by band intensities for triplicate measurements, was quantified and the

Figure 2. Probing of SAM-I Aptamer **Domain RNA Folding**

- (A) NMIA probing of magnesium-dependent changes in the SAM-I aptamer. Lanes 1-8 are in the absence of ligand, lanes 9-16 are in the presence of 1 mM SAM.
- (B) Ligand-dependent changes in apparent melting temperatures mapped on the secondary structure of SAM-I. Colors represent the difference in T_m between bound and free RNAs; positions that do not display distinct two-state melting behavior are not included.
- (C) NAIM analysis using analogs of guanine (inosine, vellow) and adenine (2AP, red; DAP, cvan) identifies specific nucleotide positions as important for folding and/or binding.

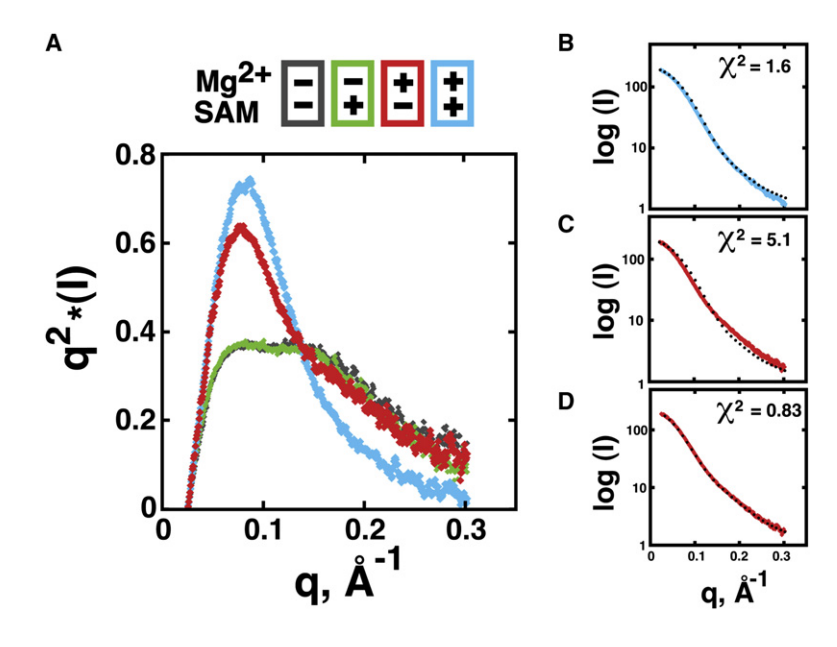
data were fit to a two-state folding transition allowing the identification of apparent melting temperatures (T_m) for most nucleotide positions in the RNA (Figure S2). Notably, the apparent T_m throughout the entire RNA increases in the presence of SAM, supporting the idea that the ligand significantly influences the stability of the global architecture of the RNA.

To reveal the influence of SAM on folding of the RNA, the difference between T_m values (ΔT_m) in the presence and absence of SAM was determined

(Figure 2B) for all measurable positions. We observe that helical regions experience the least ligand-dependent changes in T_m while elements of tertiary architecture and nucleotides comprising the SAM binding pocket experience significant ligand dependent increases in their apparent T_m (Figure 2B). The greatest changes are observed around a base triple (positions 24/64/85) that anchors J4/1 to the pseudoknot and J3/4, that displays a ${\sim}20^{\circ}\text{C}$ change in $T_{m}.$ Other regions such as J1/2 display a more moderate SAM-dependent increase T_m ($\sim 10^{\circ}$ C), a result that supports molecular dynamics simulation predictions that J1/2 docking to P3 is sensitive to magnesium (Huang et al., 2009).

Nucleotide analog interference mapping (NAIM) is another probing technique that provides specific information about functional groups critical for both folding and binding (Ryder and Strobel, 1999; Strobel, 1999). For SAM-I, RNAs that properly fold and bind ligand are selected on the basis of an observed electrophoretic mobility shift in the presence of SAM (Figure S3). RNAs rendered inactive by analog incorporation are not present in the selected population, which are analyzed by sequencing to identify sites at which a loss or gain of a single functional group in the RNA abrogates its interaction with SAM. Using three purine analogs (2-aminopurine and 2,6-diaminopurine as adenosine analogs and inosine as a guanosine analog), we observed interferences both inside and outside of the binding pocket (Figure 2C). The majority of these interferences cluster within the 24-64-85 base triple, J3/4, and the kink-turn highlighting the importance of stabilizing interactions outside of the binding pocket that are required to bind ligand in a productive manner through maintaining proper folding.





Together, these experiments identify several features critical to folding of the SAM-I riboswitch. First, while magnesium can fully stabilize some elements of tertiary architecture, primarily the pseudoknot, other key features such as the base triple tying L2, J3/4, and J4/1 together are only marginally stable in the absence of SAM. The detailed NMIA reactivity patterns suggest that in the absence of ligand, the RNA exists as an ensemble of conformations ranging from minimal tertiary structure to the bound-like state. Increasing the concentration of magnesium favors the formation of structures that are increasingly reminiscent of the SAM-bound structure. Second, it is clear that addition of ligand globally stabilizes the architecture of the RNA. While the above experiments provide a wealth of information concerning the effects of ligand and magnesium binding on RNA folding, they yield limited information about the overall architecture of the RNA, and in particular, the interhelical organization. To provide a more complete model of aptamer domain RNA folding in the absence of ligand, we have employed a small angle X-ray scattering analysis (SAXS).

Conformational Heterogeneity of P1 and P3 in the Absence of SAM Identified by SAXS

SAXS is a technique in which the scattering of X-rays is highly sensitive to the structure of the macromolecule in solution (Lipfert and Doniach, 2007; Putnam et al., 2007). Since the free state RNA samples multiple conformations in solution, we can utilize computational approaches to identify a unique set of conformational states that best describes the observed X-ray scattering profile (Putnam et al., 2007). SAXS can therefore yield an unbiased structural perspective of globally distinct conformations of the RNA in the unliganded state. SAXS data were collected on the SAM-I aptamer domain in the presence and absence of 7.6 mM magnesium and/or 100 μ M S-adenosylmethionine. To ensure the RNA sample was purely monomeric, each sample was passed through a gel filtration column immediately prior to an X-ray scattering analysis.

Figure 3. SAXS Analysis of SAM-I Solution Structure

(A) Kratky plot representation of scattering data in the presence or absence of ligand and/or magnesium.

(B) Raw scattering data of SAM-I in the presence of ligand and magnesium (blue) with the theoretical scattering curve generated from the bound state aptamer domain crystal structure superimposed (2GIS). The intensity units for (B), (C), and (D) are on a relative scale.

(C) Raw scattering data of the free state RNA in the presence of magnesium overlayed with the theoretical curve used in (B). (D) Scattering data of the free state RNA in the presence of magnesium overlayed with a theoretical scattering curve calculated from a set of structures representing frequently sampled conformations identified by an ensemble optimization algorithm (Figure 4).

The experimental SAXS data were transformed into Kratky plots to evaluate the degree of macromolecular compaction (Doniach, 2001). For all data sets, we did not observe any radiation-induced aggregation during data collection as judged by the unbiased distribution of points in the Guinier region (Figure S4). In the absence of

magnesium or SAM, the RNA displays a significant enrichment in the higher scattering angles, characteristic of an unfolded polymer in solution (Figure 3A, gray) (Doniach, 2001). This lack of compaction could not be overcome with the addition of ligand (Figure 3A; green), consistent with chemical probing data. However, in the presence of magnesium alone, there is a significant change in the scattering profile resulting in a comparable decrease in the radius of gyration (Figure 3A, red) and transition of the scattering profile into a more bell-shaped curve indicative of a folding event that shifts the RNA population toward a compacted state (Doniach, 2001). Addition of SAM and magnesium (Figure 3A; blue) further alters the profile compared to magnesium alone, indicating that although magnesium induces a large-scale global compaction in the aptamer, ligand binding also induces structural rearrangements consistent with the above chemical probing analysis.

The observed scattering profile of the RNA in the presence of magnesium and SAM is nearly identical to a theoretical scattering curve generated using the X-ray crystal structure of the bound SAM-I RNA (PDB ID 2GIS) (χ^2 = 1.6) (Figure 3B). However, the scattering profile in the presence of magnesium alone has a poor correlation (χ^2 = 5.1) to the theoretical scattering curve calculated from the crystal structure (Figure 3C). These data clearly show that the RNA collapses into a compacted state that is different from the bound X-ray structure in the presence of magnesium, but what is the molecular architecture of the states that are significantly populated in the ensemble of structures?

To model possible conformations of the aptamer domain that would be consistent with the scattering profile in the absence of SAM, torsion angle molecular dynamic simulations using the bound structure were performed. The X-ray crystal structure was divided into small discrete rigid bodies based on FIRST analysis that was further constrained by the RNA's secondary structure (Fulle and Gohlke, 2008). Regions of flexibility were chosen based on the NMIA chemical probing data to generate



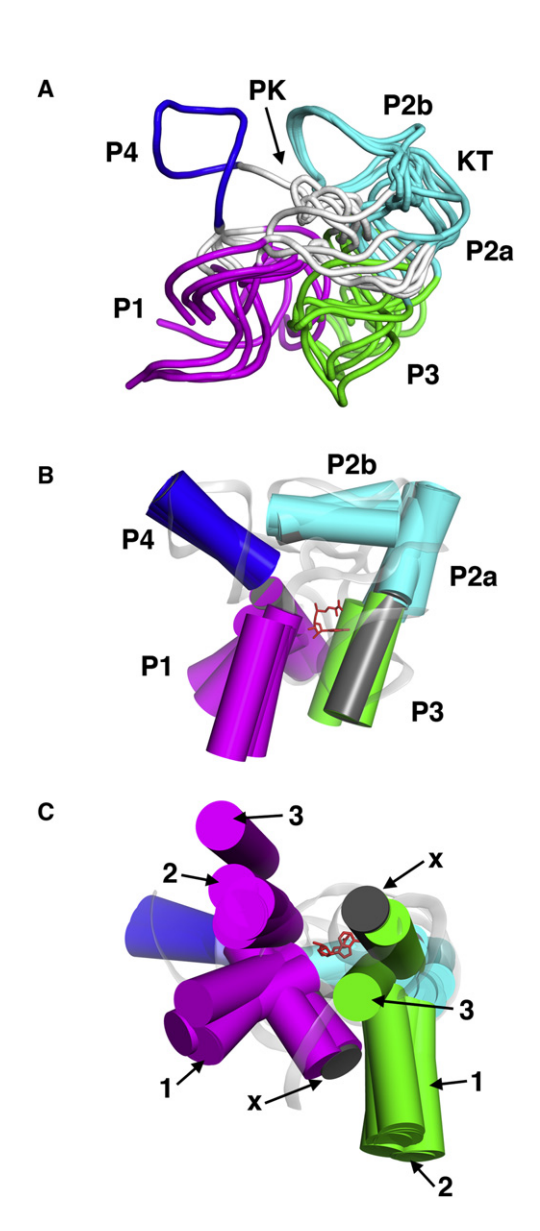


Figure 4. Ensemble of States That Generates the Best Fit to Experimental SAXS Data

(A) Overlay of the 13 free state conformations using THESEUS (Theobald and Wuttke, 2008) reveals a large conformational heterogeneity in the orientation of the P1 (magenta) and P3 (green) helical regions relative to the P4 (blue)-PK-P2a/b subdomain (cyan).

(B) Identical perspective as in (A), but helical regions are modeled as cylinders for clarity. The bound state is included in the superimposition and colored in gray both in a cylinder and ribbon representation.

(C) Bottom view of structures represented in (B) illustrating the varying degree of openness between P1 and P3 as well as the significant twist relative to the P4-PK-P2a/b subdomain. Three distinct conformational extremes (1–3) and the crystallographically identified bound state (x) are labeled accordingly.

a set of trajectories that resulted in 9000 different conformations of the RNA, and each conformation was used to calculate a theoretical scattering curve. The entire family of curves was used in an ensemble optimization algorithm against the experimental SAXS data to select the best set of conformations that modeled either the magnesium alone or magnesium/SAM SAXS data.

In the presence of magnesium and SAM, selected ensembles from the SAXS data are consistent with the bound X-ray crystal structure suggesting the solution structure of bound SAM-I is nearly identical to the X-ray crystal structure (Figure S5). However, ensemble optimization of the magnesium only SAXS data yielded a solution structure defined by multiple alternative conformations. A theoretical scattering curve generated by this ensemble of structures is in excellent agreement with the experimental data (χ^2 = 0.83) (Figure 3D). Superposition of this ensemble of structures using a maximum likelihood method (Theobald and Wuttke, 2008) clearly shows that the conformation of a subdomain consisting of P4, the pseudoknot, and P2a/b is nearly identical to the bound structure (Figure 4A). In contrast, the distance between P1 and P3 and their orientation relative to the P4-PK-P2a/b subdomain is variable and is accompanied by a significant twist relative to the bound state (Figures 4B and 4C). These structures are similar to those generated by a molecular dynamics simulation study of SAM-I aptamer that employed a purely computational approach (Huang et al., 2009). Consistent with the chemical probing data, we observe bound-like states within the ensemble where P1 and P3 are positioned as they are in the crystal structure, indicating this state is accessible in the absence of ligand.

Local Conformational Heterogeneity in the Binding Pocket

We have identified aspects of global conformational changes occurring in the free aptamer domain in response to magnesium and ligand binding; however, local conformational changes in P3, suggested by chemical probing, cannot be resolved using SAXS. To investigate structural differences between the free and bound RNA, we crystallized the SAM-I RNA in the absence of SAM and solved its structure at 2.9 Å resolution (Table 1). The global free state structure is nearly identical to the bound state (maximum likelihood rmsd is 0.12 Å over all RNA atoms) (Figure S6). This finding is consistent with the SAXS data indicating that the free RNA can sample a bound-like configuration.

At the local level, the ligand free and bound forms of the RNA are also similar, except for a significant difference within the P3 region of the SAM binding pocket (Figure 5A). In the bound state, an internal loop comprising two highly conserved nucleotides (A45 and U57) form a base triple with the adenosyl moiety of SAM while the third nucleotide (A46) is coplanar with the adjacent C47-G56 pair (Figure 5A, bottom). In the absence of ligand, A46 replaces the adenosyl moiety of SAM to form a base triple with A46 and U57. In contrast to the adenosyl moiety of SAM, which interacts with U57 via its Hoogsteen face, A46 hydrogen bonds with U57 using its Watson-Crick face (Figure 5A, top). It is important to note, however, that this structure cannot be the only one represented in solution, since A46 must be able to disengage from U57 in order for SAM to bind. Such dynamics are observed in the chemical probing reactivity pattern around these two nucleotides; in the absence of SAM both A45 and A46 show high degrees of NMIA reactivity while U57 appears to be static (Figure 2A; cf. lanes 8 and 16). Notably, when crystals of the unliganded RNA were soaked with 1 mM SAM, electron density within the binding pocket corresponding to SAM was clearly observed (Figure 6). Therefore, the crystallographically observed free state is a fully active state capable of sensing



	A94G, bound	A94G, free
ata collection	7.6.1.6, 200.1.6	7.6.7.6., 11.00
Space group	P4 ₃ 2 ₁ 2	P4 ₃ 2 ₁ 2
Cell dimensions $a = b$, c (Å); $\alpha = \beta = \gamma$ (°)	61.8, 157.6; 90	62.7, 159.2; 90
Wavelengh (Å)	1.5418	1.5418
Resolution (Å)	20 - 2.55	20 - 2.8
R _{merge} (%) ^a	5.3 (34.3)	8.2 (36.1)
I/σ(I) ^a	16.4 (4.1)	14.4 (4.4)
Completeness ^a	99.3 (99.9)	100 (99.8)
Redundancya	5.0 (4.8)	7.2 (5.5)
efinement		
Resolution (Å)	20- 2.55	20-2.9
No. reflections	18805 (1814)	13401 (1237)
R _{work} /R _{free} (%)	24.9/29.3	23.1/27.1
No. atoms		
RNA	2030	2030
Ligand/ion	35	10
Water	47	94
Mean B-factors (Ų)		
RNA	56.0	55.2
Ligand/ion	58.2	87.8
Water	35.9	45.2
rmsds		
Bond lengths (Å)	0.005	0.005
Bond angles (°)	1.14	1.22
Cross-validated Luzzati coordinate error	0.49	0.47
PDB accession code	3IQR	3IQP

SAM and implies decoupling of global P1/P3 scissoring from local opening and closing of the binding pocket in P3.

The observed positioning of A46 in the free state may be a consequence of this conformation being the most stable among all accessible conformations. Chemical probing patterns for A45 and A46 suggest each residue adopts a reactive state in the absence of ligand implying that the unconstrained reactive state is energetically accessible. In an NMR study of a very similar internal loop motif, the nucleotide equivalent to A45 was observed to be unpaired but stacked within the helix while the equivalents of A46 and U57 form a Watson-Crick pair underscoring the potential for this internal loop to adopt a multiple conformations (Popenda et al., 2008). To provide further insights into potentially accessible conformations of A45 and A46 that can be sampled in the free state, we performed replica exchange molecular dynamics (REMD) simulations (Garcia and Sanbonmatsu, 2001).

REMD is an enhanced-sampling molecular dynamics technique that allows characterization of the equilibrium thermodynamics of a system (Mitsutake et al., 2001). This method has been previously applied to understanding RNA folding (Garcia and Paschek, 2008) and motions in the ribosomal RNA (Sanbonmatsu, 2006; Vaiana and Sanbonmatsu, 2009). Simula-

tions were performed for 1.7 μ sec in explicit solvent on the region surrounding the P3 helix, including the SAM-binding site and portions of P1, P3, J1/2, J3/4, and J4/1, totaling 50 nucleotides (Movie S1). To characterize the free energy landscape, the parameter Q1 is used to describe the pairing interaction between A46 and U57 using the distance between ring nitrogen atoms as a measure of pairing (\sim 3 Å) or lack of pairing (\sim 7.5 Å). The free energy (the potential of mean force) determined by $\Delta G = -kT(log P(Q))$ is then plotted as a function of Q1 (Figure 5B; black). A second parameter, Q2, is also considered (Figure S7) that reflects stacking between A45 and A46.

The energy landscape displays three conformational basins where the closed A46 conformation (C-A46) observed in the free state crystal structure and the open conformation (O-A46) observed in the bound state are observed as local energy minima. These minima are separated by a sufficiently low energy barrier such that in the absence of SAM these are the dominant conformers. A third subtle intermediate state was also identified that occupies a shallow energy well between the closed and open energy basins (Figure 5B; asterisk). We note that transitions between basins occur often during the simulations; however, the closed A46 state is more stable than the open state by approximately 1–2 kcal/mol with an activation energy barrier of $\sim\!\!2-3$ kcal/mol. This suggests that the closed and open A46 states are rapidly sampled by the SAM binding pocket.

As a further measure of the importance of position 46, we refer to the NAIM analysis (Figure 2C). Incorporation of either 2-aminopurine (2AP) or 2,6-diaminopurine (DAP) at positions 45 and 46 is detrimental to formation of the ligand-induced electrophoretic gel shift. In each case, addition of a 2-amino group is deleterious to SAM binding. Interference of DAP and 2AP at the 100% conserved position 45 is likely the result of a steric clash with SAM, thereby directly preventing binding. However, the effect at position 46 is more difficult to explain, especially in light of the fact that guanosine is tolerated in 12% of the $\sim\!1200$ known sequences (pyrimidine residues are never observed at this position) (Griffiths-Jones et al., 2003).

Based upon these data, a second REMD simulation (Movie S2) was performed in which A46 was replaced with (DAP) (Figure 5B; red). One hypothesis is that the 2-amino group of DAP might stabilize the closed A46 state by allowing an additional hydrogen bond with U57. Upon REMD characterization of the closed A46 to open A46 transition, we observe that the DAP is more stable than the wild-type sequence ($\Delta\Delta G \sim 1~\text{kcal/mol})$ with a difference in activation barriers for collapsed to extended transition of \sim 1-2 kcal/mol (when considering both Q1 and Q2) (Figure S7). Together, the above experiments further highlight the importance of inherent conformational sampling in the free-state RNA and how subtle sequence alterations can reshape the folding landscape.

DISCUSSION

The coupling of RNA folding and ligand binding is central to regulating gene expression by riboswitches. A critical folding branch-point is established immediately after the aptamer domain is transcribed since this is the domain that actively interrogates cellular metabolite concentrations. To act as an effective transcriptional regulator, the aptamer domain must rapidly fold while avoiding misfolding or nonproductive kinetic traps to allow



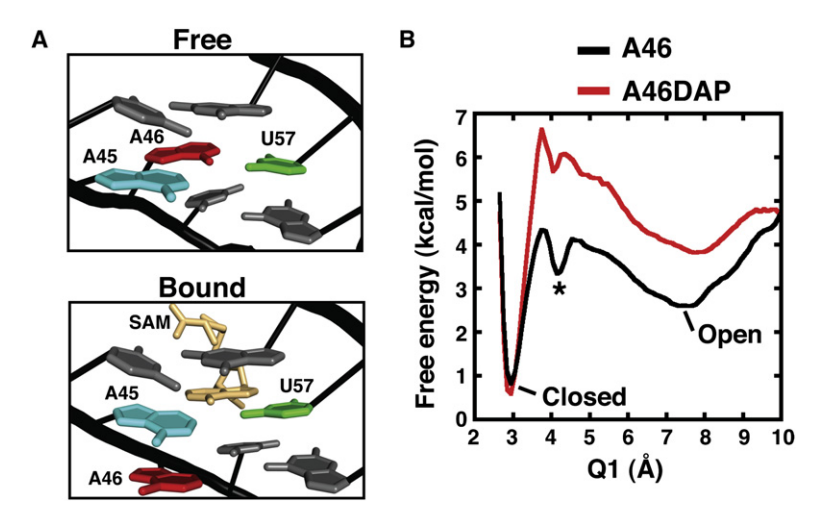


Figure 5. X-ray Crystal Structure and REMD Analysis of the Free Aptamer

(A) In the free RNA (top), a base triple between the three nucleotides that define the internal loop (A45, A46, and U57) is observed. In association with SAM (yellow), A46 is flipped out of the A45/U57 plane placing it in the minor groove adjacent to the C47-G56 pair (bottom).

(B) Free energy landscape from REMD simulations of binding region using the free and bound crystal structures as initial states. The conformation of the internal loop is described by Q1, which characterizes the base pair hydrogen bond distance between A46 and U57. Two major energy minima are observed representing the closed (free) (~3 Å) and open (bound) (~7.5 Å) states as well as a subtle intermediate state (asterisk, ~4 Å).

specific, high-affinity ligand binding. The free state must also be capable of directing the mRNA down one of two folding pathways depending upon whether it binds the appropriate ligand (Figure 1A). This latter requirement implies that the aptamer domain adopts a metastable folding landscape that allows access to multiple folding states rather than a single free state, a critical feature that confers activity in RNAs and proteins by allowing reversible sampling of states that are of comparable

stabilities (Boehr et al., 2009; Henzler-Wildman and Kern, 2007; Munro et al., 2009).

The free state aptamer domain is characterized by an ensemble of states that experience global and local conformational sampling rather than adopting a single, highly populated state. In the absence of magnesium and ligand, only elements of secondary structure are established resulting in a conformationally unrestricted ensemble in the folding phase

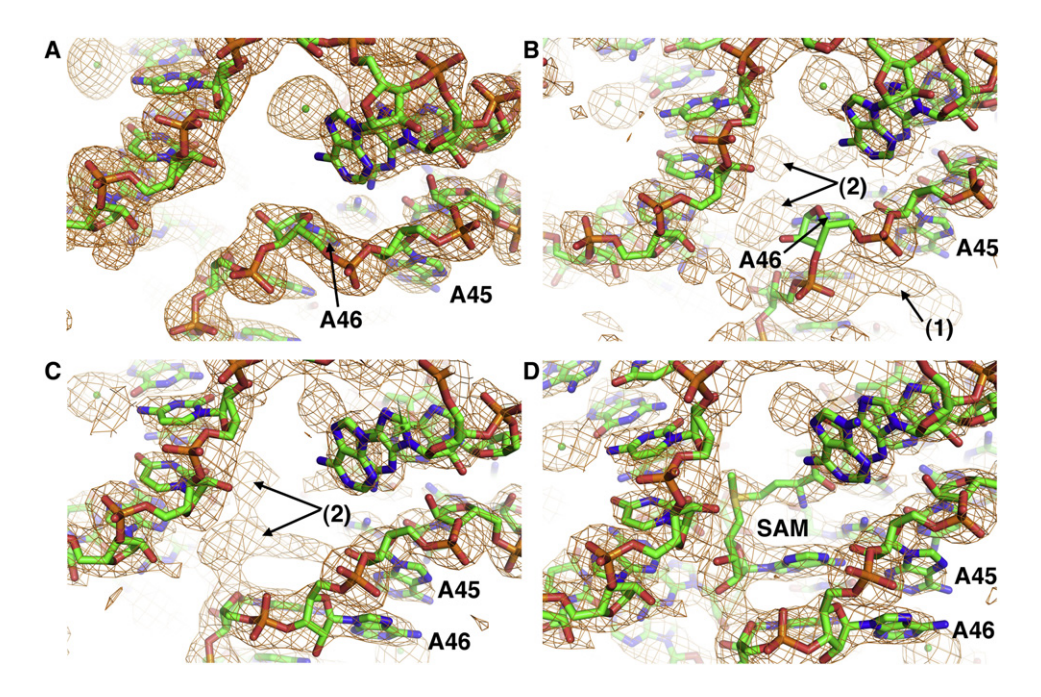


Figure 6. Soak of apo-Crystal with SAM

(A) $2F_0$ - F_0 map of the unliganded aptamer with the final model (PDB 3IQP) superimposed.

(B) 2Fo-Fc map of the SAM-soaked apo-crystal in which the free state RNA was used as the model. Note extra density corresponding to the position of A46 (1) and SAM (2) in the bound structure.

(C) 2Fo-Fc map of the same SAM soaked crystal in which the bound RNA (3IQR) was used as the model. Note that A46 is now well defined by density, and there still is unaccounted for density in the SAM binding pocket.

(D) 2Fo-Fo map of the same crystal in which the bound RNA and SAM was used as the search model. The density around SAM is well defined indicating the presence of ligand.



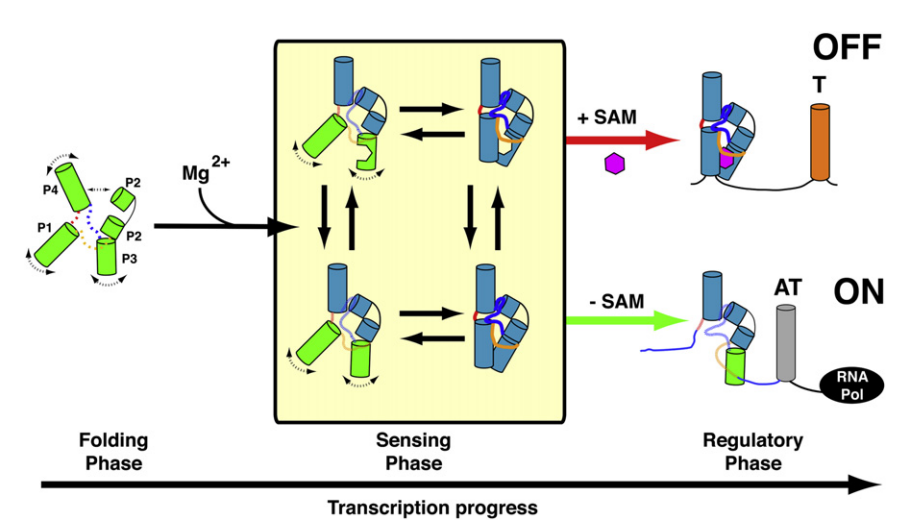


Figure 7. Model of Magnesium and Ligand Dependent Folding in a Transcriptionally Controlled SAM-I Riboswitch

Magnesium binding initiates a collapse from a form with only established secondary structure (far left) to a conformationally restricted ensemble of structures characterized by formation of the P4-PK-P2a/b subdomain. During the sensing phase. the aptamer rapidly samples conformations on both the global (scissoring of P1/P3) occurs and local (SAM binding pocket) levels (yellow box). Productive interactions with SAM result in the RNA following a folding pathway that results in formation of a terminator stem that terminates transcription (top). In the absence of ligand binding, a folding pathway is followed where the 3' side of P1 is free to form alternative pairing interactions thus establishing the antiterminator stem and allows transcription to proceed (bottom).

that is not competent to bind ligand (Figure 7). Addition of magnesium induces formation of the pseudoknot interaction, establishing a conformationally restricted ensemble that is competent to bind ligand thus establishing the sensing phase. Although this ensemble is characterized by an established P4-PK-P2a/b subdomain, the P1 and P3 helical regions sample a series of states via a "scissoring" motion that varies in the degree of displacement of one helix from the other (Figure 4). This motion allows the aptamer access to a state that is structurally similar to the SAM-bound structure in the absence of ligand binding suggesting the energetic barriers between states in the sensing phase are easily traversed. The bound-like state is competent to bind ligand, and the propensity to access this state is increased under elevated magnesium conditions; however, ligand binding is required to completely shift a population of RNAs to a homogeneous, fully structured state. From an induced-fit binding model perspective (Leulliot and Varani, 2001; Williamson, 2000), ligand captures a near-native state (conformational capture) followed by limited conformational changes to adopt the fully "native" state. This view is consistent with previous observations of the purine riboswitch (Ottink et al., 2007; Stoddard et al., 2008).

Concurrent with global conformational changes are alterations in local pairing interactions within the critical internal loop in P3, which comprises a crucial part of the SAM binding pocket. The internal loop that binds the adenosyl moiety of SAM experiences at least two distinct equilibrium conformations, dominated by the closed and open A46 states (Figure 7) that likely prevent the binding pocket from permanently collapsing into a state that is incompetent to bind ligand. Structural heterogeneity has been observed previously within similar internal loop compositions (Popenda et al., 2008), indicating that positioning two adenosine bases adjacent from an unpaired uridine may confer a unique pairing equilibrium that allows conformational sampling and may explain phylogenetic conservation trends. Notably, sampling of global and local structures are decoupled in the free state RNA, potentially allowing multiple folding pathways that lead to a unique folding outcome. The maintenance of conformational heterogeneity within the free state SAM-I RNA is compatible with our current understanding of riboswitch-mediated gene regulation. In the free state of the aptamer domain, the RNA must be sufficiently structured to ensure productive interactions with ligand, yet also be partially unstructured to allow the default folding pathway to occur with high fidelity in the absence of ligand. Limiting conformational heterogeneity through the establishment of tertiary interactions selectively populates bound-like or binding competent states, which likely has a significant impact on the rate of binding, a critical parameter for riboswitch function (Wickiser et al., 2005). This process likely explains how the SAM-I riboswitch can be tuned to respond to differing concentrations of ligand in the same organism such that it can differentially control operons related to diverse aspects of sulfur metabolism (Tomsic et al., 2008). Small alterations in aptamer sequence could alter how the RNA populates the ensemble thereby changing its responsiveness. Weakening tertiary interactions in the P4-PK-P2a/b subdomain would allow the riboswitch to respond at elevated SAM concentrations relative to other SAM-I riboswitches in the same organism.

Most other classes of riboswitches are very likely to employ conformational sampling of an ensemble of states to control their switching behavior. While different classes of riboswitches appear to behave differently (Baird and Ferre-D'Amare, 2010), their idiosyncrasies are a result of studying each RNA under varying magnesium, temperature, and ligand conditions. In addition, many of these studies have employed diverse phylogenetic variants that evolved to function under different cellular conditions. In the context of the cell and transcription, each individual riboswitch is likely tuned to populate an ensemble that includes near-native states in a fashion that meets the regulatory needs of a specific set of genes. Given the importance of dynamic conformational ensembles in a broad array of biological processes involving recognition (Boehr et al., 2009), it is not surprising that riboswitches use this as central means of coupling ligand binding to regulatory control.

EXPERIMENTAL PROCEDURES

RNA Preparation

DNA templates for transcription reactions were synthesized using complementary overlapping oligonucleotides (Integrated DNA Technologies, Inc.)



by PCR. RNA was transcribed and purified using methods previously described (Montange and Batey, 2006).

Selective 2' Hydroxyl Acylation Analyzed by Primer Extension

Reactions were performed in a modified format similar to that previously described (Stoddard et al., 2008). Modifications were initiated with 65 mM NMIA at a final concentration of 200 µM S-adenosylmethionine (Sigma-Aldrich) or with anhydrous DMSO (Sigma-Aldrich) for negative control reactions. Primer extension reactions were allowed to proceed for 7 min. Data were analyzed as previously described (Stoddard et al., 2008) except for the PK interaction where the data were separated into to transitions and fit individually.

Nucleotide analog Interference Mapping

Phosphorothioate nucleotide analogs (Glen Research) were incorporated into RNA transcripts using previously described protocols (Ryder et al., 2000). Reactions containing RNA with and without 75 μM SAM were prepared in a buffer containing 250 mM Tris-HCl (pH 7.4), 10 mM MgCl₂, 500 mM KCl. Selection of SAM bound and free conformations was performed by separation on a native polyacrylamide gel (8% polyacrylamide, 0.5× TBE, 1.1 mM MgCl₂) at 18°C. For sequencing, the RNA was end labeled by ligating a sevennucleotide DNA oligomer with an attached 3'-Alexafluor 488 (Molecular

Analysis was performed on an ABI Prism 310 Genetic Analyzer capillary electrophoresis system (National Stable Isotope Resource facility, LANL). Samples were resuspended in 5 μl 10 mM l_2 in deionized formamide, heated to 90°C for 2 min, diluted to 16 μl with formamide, and loaded on the sequencer. Control samples for nonspecific cleavage were performed for each without iodine cleavage. Fluorescence electropherograms were plotted with Origin 7, and, after normalizing for variability in electrokinetic injection, sites of interference identified by the lack of a peak at the residue in the SAM-bound versus free samples.

Small-Angle X-ray Scattering

Chromatographic separation of the RNA by gel filtration and analysis by multiangle light scattering (MALS) was performed as previously described (Rambo and Tainer, 2010). SAXS experiments were performed at Beamline 12.3.1 of the Advanced Light Source, Lawrence Berkeley National Lab, Twenty microliters of purified RNA samples and corresponding flow-through buffers from the size-exclusion purifications were loaded into a 96-well plate. RNA samples were collected at a maximum concentration of 2-3 mg/ml and diluted serially in the plate. Sample loading and data collection is as described (Hura et al., 2009). All data collections were performed at room temperature. For each sample, three exposures were taken in the following order of 6, 60, and 6 s. The first and last 6 s exposures were directly overlaid to visually assess the potential for radiation damage.

The merging of the 6 and 60 s exposures and the overlays of the merged datasets were performed with PRIMUS (Konarev et al., 2003). Kratky plots were generated with Kaliedegraph. A graph theory analysis of the X-ray crystal structure 2GIS as implemented in the program FIRST was used to determine which regions of the RNA were most likely to be flexible or stiff. Information was compiled with the established secondary structure to determine a set of rigid body modeling constraints for torsion angle molecular dynamic simulations by CNS (Brunger et al., 1998). The simulations were performed with large time steps and no electrostatic potential in the force field calculation. Any variation in the initial constraints created a unique trajectory and final state of the RNA. The conformation of the RNA at each time step along a trajectory was written to a PDB file using VMD. All SAXS calculations from X-ray models were performed with CRYSOL using a solvent density of 0.334 electrons/A3 and solvent layer of 3Å (Svergun et al., 1995).

The fit between theoretical and experimental scattering curves was assessed using χ^2 as defined by:

$$\chi^2 = \frac{1}{N-1} * \sum \left(\frac{I_{obs}(q) - c * I_{molel}(q)}{error(I_{obs}(q))} \right)^2,$$

where c is a scaling factor, I_{obs} is the observed intensities, I_{model} is the modeled SAXS intensities, and error(I_{obs}) is the measured error in I_{obs} . Assuming the experimental data are accurate and free of gross errors, an atomistic model with a χ^2 of less than 2 is generally considered to be a model consistent with the experimental SAXS data. If a model produces a χ^2 between 2 and 3, then the model is considered a poor model. More importantly, a meaningful value of χ^2 is determined by noting that the putative model has a radiusof-gyration consistent with the data and that the fit of the model to the experimental data is evenly distributed typically confined to the lower angle scattering region (q < 0.2).

The final ensemble of conformers selected by EOM (Bernado et al., 2007) using the magnesium alone data consists of 13 members that cluster into two major groups: opened (11 members) and closed (2 members). Of the 11 opened members, they could be further reduced to four types of closely related structures, and therefore the small overfitting of the data, as indicated by a χ^2 below 1, is due to the redundancy found in the selected members. EOM does not determine the optimal ensemble size and the value of χ^2 can be artificially raised by arbitrarily pruning redundant members. However, to ensure the reproducibility of the results, we have chosen not to do so and present the full EOM-selected ensemble.

X-ray Crystallography

Crystallographic models of the free state RNA were generated in a manner previously described (Montange and Batey, 2006; Montange et al., 2010). Ligand soaking experiments were performed with unbound crystals grown at 20°C. Crystals were washed three times with 10 μl mother liquor followed by three times with mother liquor supplemented with 0.5 mM S-adenosylmethionine. After washing, crystals were soaked in 6 μ l SAM-supplemented mother liquor at 20°C for 24 hr followed by cryoprotection as described below in solutions containing no SAM. All crystals were cryoprotected in mother liquor supplemented with 15% ethylene glycol with a 5 min soak and flashfrozen in liquid nitrogen. Data were collected using a rotating copper anode X-ray source with an R-AXIS IV++ area detector (Rigaku). Data were indexed, scaled, and averaged using CrystalClear (Pflugrath, 1999), and the models were refined in CNS (Brunger et al., 1998). Crystallographic data and refinement statistics are given in Table 1.

Replica Exchange Molecular Dynamics Simulations

In replica exchange molecular dynamics (REMD), a distribution of identical systems are simulated at different temperatures. When favorable, temperatures are exchanged between neighboring replica systems according to a Monte Carlo criterion, resulting in Boltzmann sampling. In a previous study of a similarly sized RNA system, convergence of the free energy landscape was obtained after approximately 1 µsec of total sampling (Vaiana and Sanbonmatsu, 2009). We use a similar simulation strategy, including 48 replicas with temperatures 3.5°C (276.5 K) < T < 174.5°C (447.5 K), running on 384 processors of the LANL Coyote supercomputer, generating a total sampling of 1.7 μsec . The simulations were performed in explicit solvent using particle mesh Ewald electrostatics and the Gromacs simulation code. The free energy is calculated using the potential of mean force $\Delta G = -kT \log (P(Q))$, where P(Q)is the probability of sampling state characterized by coordinate Q, P(Q) = N(Q)/ N_{tot} , N(Q) is the number of states in configuration Q sampled during the simulation, and N_{tot} is total number of configurations sampled. The coordinate values Q1 and Q2 are defined as:

$$Q2 = (distance(A45 \ N1 \ .. \ A46 \ N1) + distance(A45 \ N6 \ .. \ A46 \ N6))/2.$$

REMD simulations also provide the temperature dependence of $\Delta G(a,b,T)$, used here to separate enthalpic and entropic contributions to the free energy at $T_0 = 27^{\circ}$ C (300 K) for dissociation of S-adenosylmethionine from the binding site.

ACCESSION NUMBERS

Coordinates and structure factors for the SAM-I A94G variant RNA free and in complex with SAM have been deposited to the RCSB with accession numbers 3IQP and 3IQR, respectively.



SUPPLEMENTAL INFORMATION

Supplemental Information includes seven figures and two movies and can be found with this article online at doi:10.1016/j.str.2010.04.006.

ACKNOWLEDGMENTS

This work was supported by National Institutes of Health grant GM083953 (to R.T.B.), the Los Alamos National Laboratories LDRD program, and NIH ARRA RC1GM092031 (to K.Y.S). Support for data collection at the Lawrence Berkeley National Laboratory SIBYLS beamline of the Advanced Light Source came from the DOE program Integrated Diffraction Analysis Technologies (IDAT) under Contract DE-AC02-05CH11231 with the U.S. Department of Energy. In this study, C.D.S. performed the chemical probing analysis, R.K.M. performed the crystallography, S.P.H. performed the NAIM experiments at LANL, S.P.H. and K.Y.S. performed REMD simulations, and R.P.R. performed the SAXS analysis. C.D.S. and R.T.B. wrote the paper with input from all authors

Received: February 9, 2010 Revised: March 31, 2010 Accepted: April 3, 2010 Published: July 13, 2010

REFERENCES

Baird, N.J., and Ferre-D'Amare, A.R. (2010). Idiosyncratically tuned switching behavior of riboswitch aptamer domains revealed by comparative small-angle X-ray scattering analysis. RNA 16, 598–609.

Barrick, J.E., and Breaker, R.R. (2007). The distributions, mechanisms, and structures of metabolite-binding riboswitches. Genome Biol. 8, R239.

Bernado, P., Mylonas, E., Petoukhov, M.V., Blackledge, M., and Svergun, D.I. (2007). Structural characterization of flexible proteins using small-angle X-ray scattering. J. Am. Chem. Soc. 129, 5656–5664.

Boehr, D.D., Nussinov, R., and Wright, P.E. (2009). The role of dynamic conformational ensembles in biomolecular recognition. Nat. Chem. Biol. *5*, 789–796.

Brunger, A.T., Adams, P.D., Clore, G.M., DeLano, W.L., Gros, P., Grosse-Kunstleve, R.W., Jiang, J.S., Kuszewski, J., Nilges, M., Pannu, N.S., et al. (1998). Crystallography & NMR system: a new software suite for macromolecular structure determination. Acta Crystallogr. D Biol. Crystallogr. *54*, 905–921.

Doniach, S. (2001). Changes in biomolecular conformation seen by small angle X-ray scattering. Chem. Rev. 101, 1763–1778.

Epshtein, V., Mironov, A.S., and Nudler, E. (2003). The riboswitch-mediated control of sulfur metabolism in bacteria. Proc. Natl. Acad. Sci. USA *100*, 5052–5056.

Fulle, S., and Gohlke, H. (2008). Analyzing the flexibility of RNA structures by constraint counting. Biophys. J. 94, 4202–4219.

Garcia, A.E., and Sanbonmatsu, K.Y. (2001). Exploring the energy landscape of a beta hairpin in explicit solvent. Proteins 42, 345–354.

Garcia, A.E., and Paschek, D. (2008). Simulation of the pressure and temperature folding/unfolding equilibrium of a small RNA hairpin. J. Am. Chem. Soc. 130. 815–817.

Garst, A.D., and Batey, R.T. (2009). A switch in time: detailing the life of a riboswitch. Biochim. Biophys. Acta *1789*, 584–591.

Garst, A.D., Heroux, A., Rambo, R.P., and Batey, R.T. (2008). Crystal structure of the lysine riboswitch regulatory mRNA element. J. Biol. Chem. 283, 22347–22351.

Gherghe, C.M., Shajani, Z., Wilkinson, K.A., Varani, G., and Weeks, K.M. (2008). Strong correlation between SHAPE chemistry and the generalized NMR order parameter (S2) in RNA. J. Am. Chem. Soc. *130*, 12244–12245.

Gilbert, S.D., Stoddard, C.D., Wise, S.J., and Batey, R.T. (2006). Thermodynamic and kinetic characterization of ligand binding to the purine riboswitch aptamer domain. J. Mol. Biol. 359, 754–768.

Griffiths-Jones, S., Bateman, A., Marshall, M., Khanna, A., and Eddy, S.R. (2003). Rfam: an RNA family database. Nucleic Acids Res. *31*, 439–441.

Grundy, F.J., and Henkin, T.M. (1998). The S box regulon: a new global transcription termination control system for methionine and cysteine biosynthesis genes in gram-positive bacteria. Mol. Microbiol. *30*, 737–749.

Henzler-Wildman, K., and Kern, D. (2007). Dynamic personalities of proteins. Nature 450, 964–972.

Heppell, B., and Lafontaine, D.A. (2008). Folding of the SAM aptamer is determined by the formation of a K-turn-dependent pseudoknot. Biochemistry 47, 1490–1499.

Huang, W., Kim, J., Jha, S., and Aboul-ela, F. (2009). A mechanism for S-adenosyl methionine assisted formation of a riboswitch conformation: a small molecule with a strong arm. Nucleic Acids Res. 37, 6528–6539.

Hura, G.L., Menon, A.L., Hammel, M., Rambo, R.P., Poole, F.L.I.I., Tsutakawa, S.E., Jenney, F.E., Jr., Classen, S., Frankel, K.A., Hopkins, R.C., et al. (2009). Robust, high-throughput solution structural analyses by small angle X-ray scattering (SAXS). Nat. Methods 6, 606–612.

Kang, M., Peterson, R., and Feigon, J. (2009). Structural insights into riboswitch control of the biosynthesis of queuosine, a modified nucleotide found in the anticodon of tRNA. Mol. Cell 33, 784–790.

Konarev, P.V., Volkov, V.V., Sokolova, A.V., Koch, M.H.J., and Svergun, D.I. (2003). PRIMUS: a Windows PC-based system for small-angle scattering data analysis. J. Appl. Crystallogr. *36*, 1277–1282.

Leulliot, N., and Varani, G. (2001). Current topics in RNA-protein recognition: control of specificity and biological function through induced fit and conformational capture. Biochemistry 40, 7947–7956.

Lipfert, J., and Doniach, S. (2007). Small-angle X-ray scattering from RNA, proteins, and protein complexes. Annu. Rev. Biophys. Biomol. Struct. *36*, 307–327.

Loh, E., Dussurget, O., Gripenland, J., Vaitkevicius, K., Tiensuu, T., Mandin, P., Repoila, F., Buchrieser, C., Cossart, P., and Johansson, J. (2009). A transacting riboswitch controls expression of the virulence regulator PrfA in listeria monocytogenes. Cell *139*, 770–779.

McDaniel, B.A., Grundy, F.J., and Henkin, T.M. (2005). A tertiary structural element in S box leader RNAs is required for S-adenosylmethionine-directed transcription termination. Mol. Microbiol. *57*, 1008–1021.

Merino, E.J., Wilkinson, K.A., Coughlan, J.L., and Weeks, K.M. (2005). RNA structure analysis at single nucleotide resolution by selective 2'-hydroxyl acylation and primer extension (SHAPE). J. Am. Chem. Soc. 127, 4223–4231.

Mitsutake, A., Sugita, Y., and Okamoto, Y. (2001). Generalized-ensemble algorithms for molecular simulations of biopolymers. Biopolymers *60*, 96–123.

Montange, R.K., and Batey, R.T. (2006). Structure of the S-adenosylmethionine riboswitch regulatory mRNA element. Nature 441, 1172–1175.

Montange, R.K., and Batey, R.T. (2008). Riboswitches: emerging themes in RNA structure and function. Annu. Rev. Biophys. *37*, 117–133.

Montange, R.K., Mondragon, E., van Tyne, D., Garst, A.D., Ceres, P., and Batey, R.T. (2010). Discrimination between closely related cellular metabolites by the SAM-I riboswitch. J. Mol. Biol. 396, 761–772.

Munro, J.B., Sanbonmatsu, K.Y., Spahn, C.M., and Blanchard, S.C. (2009). Navigating the ribosome's metastable energy landscape. Trends Biochem. Sci. *34*, 390–400.

Ottink, O.M., Rampersad, S.M., Tessari, M., Zaman, G.J., Heus, H.A., and Wijmenga, S.S. (2007). Ligand-induced folding of the guanine-sensing riboswitch is controlled by a combined predetermined induced fit mechanism. RNA *13*, 2202–2212.

Pflugrath, J.W. (1999). The finer things in X-ray diffraction data collection. Acta Crystallogr. D Biol. Crystallogr. 55. 1718–1725.

Popenda, L., Adamiak, R.W., and Gdaniec, Z. (2008). Bulged adenosine influence on the RNA duplex conformation in solution. Biochemistry 47, 5059–5067.

Priyakumar, U.D., and Mackerell, A.D., Jr. (2009). Role of the adenine ligand on the stabilization of the secondary and tertiary interactions in the adenine riboswitch. J. Mol. Biol. 396, 1422–1438.

Putnam, C.D., Hammel, M., Hura, G.L., and Tainer, J.A. (2007). X-ray solution scattering (SAXS) combined with crystallography and computation: defining

Structure

Conformational Sampling by the SAM-I Aptamer



accurate macromolecular structures, conformations and assemblies in solution, Q. Rev. Biophys. 40, 191-285.

Rambo, R.P., and Tainer, J.A. (2010). Improving small-angle X-ray scattering data for structural analyses of the RNA world. RNA 16, 638-646.

Roth, A., and Breaker, R.R. (2009). The structural and functional diversity of metabolite-binding riboswitches. Annu. Rev. Biochem. 78, 305-334.

Ryder, S.P., and Strobel, S.A. (1999). Nucleotide analog interference mapping. Methods 18, 38-50.

Ryder, S.P., Ortoleva-Donnelly, L., Kosek, A.B., and Strobel, S.A. (2000). Chemical probing of RNA by nucleotide analog interference mapping. Methods Enzymol. 317, 92-109.

Sanbonmatsu, K.Y. (2006). Energy landscape of the ribosomal decoding center. Biochimie 88, 1053-1059.

Serganov, A., Huang, L., and Patel, D.J. (2008). Structural insights into amino acid binding and gene control by a lysine riboswitch. Nature 455, 1263-1267.

Sharma, M., Bulusu, G., and Mitra, A. (2009). MD simulations of ligand-bound and ligand-free aptamer: molecular level insights into the binding and switching mechanism of the add A-riboswitch. RNA 15, 1673-1692.

Stoddard, C.D., and Batey, R.T. (2006). Mix-and-match riboswitches. ACS Chem. Biol. 1, 751-754.

Stoddard, C.D., Gilbert, S.D., and Batey, R.T. (2008). Ligand-dependent folding of the three-way junction in the purine riboswitch. RNA 14, 675-684.

Strobel, S.A. (1999). A chemogenetic approach to RNA function/structure analysis. Curr. Opin. Struct. Biol. 9, 346-352.

Sudarsan, N., Wickiser, J.K., Nakamura, S., Ebert, M.S., and Breaker, R.R. (2003). An mRNA structure in bacteria that controls gene expression by binding lysine. Genes Dev. 17, 2688-2697.

Svergun, D., Barberato, C., and Koch, M.H.J. (1995). CRYSOL-a program to evaluate x-ray solution scattering of biological macromolecules from atomic coordinates. J. Appl. Crystallogr. 28, 768-773.

Theobald, D.L., and Wuttke, D.S. (2008). Accurate structural correlations from maximum likelihood superpositions. PLoS Comput. Biol. 4, e43. 10.1371/journal.pcbi.0040043.

Tomsic, J., McDaniel, B.A., Grundy, F.J., and Henkin, T.M. (2008). Natural variability in S-adenosylmethionine (SAM)-dependent riboswitches: S-box elements in bacillus subtilis exhibit differential sensitivity to SAM in vivo and in vitro. J. Bacteriol. 190, 823-833.

Vaiana, A.C., and Sanbonmatsu, K.Y. (2009). Stochastic gating and drug-ribosome interactions. J. Mol. Biol. 386, 648-661.

Villa, A., Wohnert, J., and Stock, G. (2009). Molecular dynamics simulation study of the binding of purine bases to the aptamer domain of the quanine sensing riboswitch. Nucleic Acids Res. 37, 4774-4786.

Wickiser, J.K., Winkler, W.C., Breaker, R.R., and Crothers, D.M. (2005). The speed of RNA transcription and metabolite binding kinetics operate an FMN riboswitch. Mol. Cell 18, 49-60.

Wilkinson, K.A., Merino, E.J., and Weeks, K.M. (2006). Selective 2'-hydroxyl acylation analyzed by primer extension (SHAPE): quantitative RNA structure analysis at single nucleotide resolution. Nat. Protoc. 1, 1610-1616.

Williamson, J.R. (2000). Induced fit in RNA-protein recognition. Nat. Struct. Biol. 7, 834-837.

Winkler, W.C., Nahvi, A., Sudarsan, N., Barrick, J.E., and Breaker, R.R. (2003). An mRNA structure that controls gene expression by binding S-adenosylmethionine. Nat. Struct. Biol. 10, 701-707.

Zhang, Q., Stelzer, A.C., Fisher, C.K., and Al-Hashimi, H.M. (2007). Visualizing spatially correlated dynamics that directs RNA conformational transitions. Nature 450, 1263-1267.